Stepwise Disintegration of the Photosynthetic Oxygen-Evolving Complex

Cecilia Tommos,[†,‡,§] John McCracken,[†] Stenbjörn Styring,[#] and Gerald T. Babcock*[,†]

Contribution from the Department of Chemistry, Michigan State University, East Lansing, Michigan 48824, Department of Biochemistry, Arrhenius Laboratories for Natural Sciences, Stockholm University, S-10691 Stockholm, Sweden, and Department of Biochemistry, Center for Chemistry and Chemical Engineering, Lund University, S-22100 Lund, Sweden

Received January 26, 1998

Abstract: Photosynthetic water oxidation catalyzed by Photosystem II takes place at a site that comprises a redox-active tyrosine, Y_Z, a tetramanganese cluster, and, in addition to its redox components, two inorganic cofactors, calcium and chloride. Recent work suggests that Y_Z and the metal site are intimately linked in the oxidation and deprotonation reactions of substrate water. The metal cluster stores oxidizing equivalents and provides binding sites for the substrate from which $Y_Z^{\bullet}$ is proposed to abstract hydrogen atoms during the catalytic cycle of photosystem II. Intrinsic to this hydrogen-abstraction mechanism for water oxidation is an intimate structural and functional relationship between the metal site and Y_Z, which predicts that the local Y_Z environment will be sensitive to the composition and integrity of the metal cluster. To test this postulate, we have examined the Y_Z site and its status with respect to solvent exposure under varying degrees of disassembly of the oxygen-evolving complex. $^1H\backslash^2H$-isotope exchange was carried out for various times in samples devoid of Mn, Ca^{2+}, and Cl^-, and in samples depleted exclusively of Ca^{2+}. The $Y_Z^{\bullet}$ and $S_2Y_Z^{\bullet}$ species were cryotrapped to high yield in these two preparations, respectively, and the radical site was characterized by using electron spin−echo envelope modulation spectroscopy. The isotope exchange at the Y_Z site was completed with an upper limit on the minutes time scale in both the $(Mn)_4$-depleted and the Ca-depleted samples. The number of isotope-exchangeable protons in the site and their distances to $Y_Z^{\bullet}$ were found to be different in the two systems, indicating that Y_Z is shielded from the solvent in the Ca-depleted system and, upon removal of the $(Mn)_4$ cluster, becomes accessible to bulk water. The results from an electron spin−echo analysis of $S_2Y_Z^{\bullet}$, in the weak-coupling limit, suggest that $Y_Z^{\bullet}$ in samples that retain the $(Mn)_4$ cluster, but lack Ca^{2+}, is involved in a bifurcated hydrogen bond. The data for both classes of samples are consistent with a hydrogen-abstraction function for Y_Z in water oxidation and provide insight into the light-driven assembly of the $(Mn)_4$ cluster.

Introduction

Photosystem II (PSII) catalyzes the oxidation of water to dioxygen in plants and algae.[1−4] The water-splitting reactions are thermodynamically driven by the light-induced oxidation of the reaction-center chlorophyll complex, P_{680}. A tetramanganese cluster[2,5] and Y_Z, a redox-active tyrosine identified as D1-Y161,[6,7] comprise the catalytic core of the PSII oxygen-evolving complex (OEC). The $(Mn)_4$ cluster binds substrate water, and by cycling through five redox states, denoted S_0−S_4, accumulates the oxidizing potential required for the catalytic process. Oxidation of water occurs along a concerted pathway upon formation of S_4 and the dioxygen product is released as the system relaxes back to S_0. In addition to its redox components, PSII requires two inorganic cofactors, calcium and chloride, for function.[1,8,9] The enzyme also contains Y_D, a second redox-active tyrosine located at position D2-160.[6,10] Y_D functions as an auxiliary electron donor and is not directly involved in the water-splitting chemistry.[3,11]

Evidence has recently accumulated that indicates a more intimate role for Y_Z in the water-oxidizing chemistry than had

* Corresponding author: Michigan State University. Fax: (517) 353 1793. Phone: (517) 355 9715 ext. 258. E-mail: Babcock@cemvax.cem.msu.edu.

† Michigan State University.

‡ Stockholm University.

Lund University.

§ Present address: The Johnson Research Foundation, Department of Biochemistry and Biophysics, University of Pennsylvania, Philadelphia, PA 19104.

(1) Debus, R. J. *Biochim. Biophys. Acta* **1992**, *1102,* 269−352.

(2) Britt, R. D. In *Oxygenic Photosynthesis: The Light Reactions;* Ort, D. R., Yocum, C. F., Eds.; Kluwer Academic Publishers: The Netherlands, 1996; pp 137−164.

(3) Diner, B. A.; Babcock, G. T. In *Oxygenic Photosynthesis: The Light Reactions;* Ort, D. R., Yocum, C. F., Eds.; Kluwer Academic Publishers: The Netherlands, 1996; pp 213−247.

(4) (a) Nugent, J. H. A. *Eur. J. Biochem.* **1996**, *237,* 519−531. (b) Witt, H. T. *Ber. Bunsen-Ges. Phys. Chem.* **1996**, *100,* 1923−1942. (c) Rüttinger, W.; Dismukes, G. C. *Chem. Rev.* **1997**, *97,* 1−24.

(5) Yachandra, V. K.; Sauer, K.; Klein, M. P. *Chem. Rev.* **1996**, *96,* 2927−2950.

(6) Barry, B. A.; Babcock, G. T. *Proc. Natl. Acad. Sci. U.S.A.* **1987**, *84,* 7099−7103.

(7) (a) Debus, R. J.; Barry, B. A.; Sithole, I.; Babcock, G. T.; McIntosh, L. *Biochemistry* **1988**, *27,* 9071−9074. (b) Metz, J. G.; Nixon, P. J.; Rögner, M.; Brudvig, G. W.; Diner, B. A. *Biochemistry* **1989**, *28,* 6960−6969.

(8) (a) Yocum, C. F. *Biochim. Biophys. Acta* **1991**, *1059,* 1−15. (b) Yocum, C. F. In *Manganese Redox Enzymes;* Pecoraro, V. L., Ed.; VCH Publishers: New York, 1992; pp 71−83. (c) Boussac, A.; Rutherford, A. W. *Biochem. Soc. Trans.* **1994**, *22,* 352−358.

(9) Tommos, C.; Babcock, G. T. *Acc. Chem. Res.* **1998**, *31,* 18−25.

(10) (a) Debus, R. J.; Barry, B. A.; Babcock, G. T.; McIntosh, L. *Proc. Natl. Acad. Sci. U.S.A.* **1988**, *85,* 427−430. (b) Vermaas, W. F. J.; Rutherford, A. W.; Hansson, Ö. *Proc. Natl. Acad. Sci. U.S.A.* **1988**, *85,* 8477−8481.

(11) Babcock, G. T.; Barry, B. A.; Debus, R. J.; Hoganson, C. W.; Atamian, M.; McIntosh, L.; Sithole, I.; Yocum, C. F. *Biochemistry* **1989**, *28,* 9557−9565.

S0002-7863(98)00281-9 CCC: $15.00
Published on Web 09/23/1998

been suspected previously. These results include a comparison between the properties of $Y_Z^\bullet$ and those of $Y_D^\bullet$ that revealed pronounced differences between the two radicals.[12] In particular, upon removal of the $(Mn)_4$ cluster, the Y_Z site becomes severely perturbed, whereas the Y_D site is insensitive to the status of the metal cluster.[13] This observation was unexpected in light of the prevailing view of Y_Z as a charge-transfer interface between P_{680} and the $(Mn)_4$ cluster and its proposed remote position with respect to the metal site. Concomitant with this work, data were presented that indicated that Y_Z and the $(Mn)_4$ cluster were in closer proximity[14] than earlier estimates.[15] Finally, fast proton release initiated by Y_Z oxidation occurs on each PSII turnover,[16] which suggests a linkage between Y_Z and the protolytic chemistry associated with water oxidation.[17]

These results and several others led us to propose a metalloradical mechanism that involves Y_Z directly in the water-oxidizing chemistry and as the key component by which PSII liberates the protons produced by this process from the active site. In this model, the $(Mn)_4$ cluster provides binding sites for substrate water/hydroxide from which $Y_Z^\bullet$ abstracts hydrogen atoms upon each S-state transition.[9,12,20] The oxidizing equivalents generated in these processes are delocalized to the $(Mn)_4$ cluster, which increases the Mn valences by one upon each turnover. This model has recently been extended to include a mechanism for the oxygen−oxygen bond forming step[20d] and the involvement of the Cl^- and Ca^{2+} cofactors in the catalytic cycle.[9] Britt and co-workers have proposed a similar metalloradical model for PSII in which Y_Z is intimately involved in the oxidation and deprotonation of substrate water.[2,14,21] A difference between these two models is the pervasiveness of the $Y_Z^\bullet$-mediated hydrogen abstractions. In the model that we have developed, Y_Z performs the same proton-coupled redox chemistry on each S-state advance. In the model presented by Britt and co-workers, Y_Z is not necessarily involved in the deprotonation of substrate on all S-state transitions.[2,14b] In addition, in the model proposed by Britt's group, the reduction and protonation of $Y_Z^\bullet$ occur as a pure sequential electron/proton-transfer event while we favor a proton coupled electron-transfer pathway.[22] Both models, however, although different in the mechanistic details, postulate that an electron and a proton are transferred from the Mn/substrate unit to $Y_Z^\bullet$.

Intrinsic to these ideas on water oxidation is a close structural and function relationship between the metal site and Y_Z. To test this postulate, several recent EMR studies have examined the distance between Y_Z and $(Mn)_4$ in samples in which water oxidation is inhibited by perturbation of the Cl^- and/or Ca^{2+} cofactors.[23] In these preparations, PSII is blocked in $S_2Y_Z^\bullet$ that is characterized by an EPR spectrum, originally observed by Rutherford and co-workers,[24] which has been analyzed to derive the nature and strength of the magnetic interactions between the two spin centers. These studied converge to ∼8 Å as the center-to-center distance between Y_Z and $(Mn)_4$.[23] An important FTIR observation shows that the short distance observed in the inhibited systems may extend to the native enzyme.[25]

Here we describe a different approach to investigate the proposed integrated $(Mn)_4Y_Z$ structure that complements and extends the distance measurements. An intimate physical and functional association between the tyrosine and the metal site predicts that the Y_Z site will be sensitive to the composition and integrity of the $(Mn)_4$ cluster. The Y_Z site is disordered[12,26] and predicted to be accessible from bulk phase in the absence of the metal cluster. Accessibility to bulk solvent in this view is essential so that the Mn^{2+} and Ca^{2+} binding processes that necessarily precede photoactivation and assembly of the functional $(Mn)_4$ cluster can occur.[27] Formation of the metal cluster is liable to bring order to the catalytic site so that two, somewhat contradictory, requirements for water oxidation are met. On one hand, PSII, which turns over about 100 molecules of H_2O s^{-1} during steady-state illumination, must allow the high flux of substrate water into the site. On the other hand, the structure of the site and its protein surrounding must restrict access by external reductants, which could reduce the higher S states and compete with oxygen evolution. Finally, in addition to these accessibility and order issues, mechanistic details of the H-atom abstraction model for water oxidation predict that the hydrogen abstractor, $Y_Z^\bullet$, is involved in bifurcated hydrogen bonds at various points in the catalytic cycle (see also ref 21).[9]

Electron spin−echo envelope modulation (ESEEM) spectroscopy has the capability to test these predictions and provide

(12) Tommos, C.; Tang, X.-S.; Warncke, K.; Hoganson, C. W.; Styring, S.; McCracken, J.; Diner, B. A.; Babcock, G. T. *J. Am. Chem. Soc.* **1995**, *117*, 10325−10335.

(13) (a) Rodriquez, I. D. Ph.D. Thesis, Michigan State University, East Lansing, Michigan, 1990. (b) Espe, M. P. Ph.D. Thesis, Michigan State University, East Lansing, Michigan, 1994. (c) Rigby, S. E. J.; Maclachlan, D. J.; Nugent, J. H. A.; O′Malley, P. J. *Biochim. Biophys. Acta* **1994**, *1188*, 318−324. (d) Warncke, K.; Babcock, G. T.; McCracken J. *J. Am. Chem. Soc.* **1994**, *116*, 7332−7340.

(14) (a) Gilchrist, M. L., Jr.; Ball, J. A.; Randall, D. W.; Britt, R. D. *Proc. Natl. Acad. Sci. U.S.A.* **1995**, *92*, 9545−9549. (b) Tang, X.-S.; Randall, D. W.; Force, D. A.; Diner, B. A.; Britt, R. D. *J. Am. Chem. Soc.* **1996**, *118*, 7638−7639.

(15) (a) Hoganson, C. W.; Babcock, G. T. *Biochemistry* **1988**, *27*, 5848−5855. (b) Un, S.; Brunel, L.-C.; Brill, T. M.; Zimmermann, J.-L.; Rutherford, A. W. *Proc. Natl. Acad. Sci. U.S.A.* **1994**, *91*, 5262−5266. (c) Kodera, Y.; Hara, H.; Astashkin, A. V.; Kawamori, A.; Ono, T. *Biochim. Biophys. Acta* **1995**, *1232*, 43−51.

(16) (a) Lübbers, K.; Haumann, M.; Junge, W. *Biochim. Biophys. Acta* **1993**, *1183*, 210−214. (b) Haumann, M.; Junge, W. *Biochemistry* **1994**, *33*, 864−872. (c) Bögershausen, O.; Junge, W. *Biochim. Biophys. Acta* **1995**, *1230*, 177−185.

(17) For an alternative interpretation of these observation see refs 18 and 19.

(18) Haumann, M.; Bögershausen, O.; Cherepanov, D.; Ahlbrink, R.; Junge, W. *Photosynth. Res.* **1997**, *51*, 193−208.

(19) Ahlbrink, R.; Haumann, M.; Cherepanov, D.; Bögershausen, O.; Mulkidjanian, A.; Junge, W. *Biochemistry* **1998**, *37*, 1131−1142.

(20) (a) Hoganson, C. W.; Lydakis-Simantiris, N.; Tang, X.-S.; Tommos, C.; Warncke, K.; Babcock, G. T.; Diner, B. A.; McCracken, J.; Styring, S. *Photosynth. Res.* **1995**, *46*, 177−184. (b) Babcock, G. T. In *Photosynthesis: from Light to Biospere;* Mathis, P., Ed.; Kluwer Academic Publishers: The Netherlands, 1995; Vol. II, pp 209−215. (c) Tommos, C. Ph.D. Thesis, Stockholm University, Stockholm, Sweden, 1997. (d) Hoganson, C. W.; Babcock, G. T. *Science* **1997**, *277*, 1953−1956. (e) Tommos, C.; Hoganson, C. W.; Di Valentin, M.; Lydakis-Simantiris, N.; Dorlet, P.; Westphal, K.; Chu, H.-A.; McCracken, J.; Babcock, G. T. *Curr. Opin. Chem. Biol.* **1998**, *2*, 244−252.

(21) Force, D. A.; Randall, D. W.; Britt, R. D. *Biochemistry* **1997**, *36*, 12062−12070.

(22) Siegbahn, P. E. M.; Blomberg, M. R. A.; Crabtree, R. H. *Theor. Chem. Acc.* **1997**, *97*, 289−300.

(23) (a) MacLachlan, D. J.; Nugent, J. H. A.; Warden, J. T.; Evans, M. C. W. *Biochim. Biophys. Acta* **1994**, *1188*, 325−334. (b) Lakshmi, K. V.; Eaton, S. S.; Eaton, G. R.; Frank, H. A.; Brudvig, G. W. *J. Phys. Chem.* In press. (c) Dorlet, P.; Di Valentin M.; Babcock G. T.; McCracken J. *J. Phys. Chem.* In press. (d) Peloquin, J. M.; Campbell, K. A.; Britt, R. D. *J. Am. Chem. Soc.* **1998**, *120*, 6840−6841.

(24) Boussac, A.; Zimmermann, J.-L.; Rutherford, A. W.; Lavergne, J. *Nature* **1990**, *347*, 303−306.

(25) Noguchi, T.; Inoue, Y.; Tang, X.-S. *Biochemistry* **1997**, *36*, 14705−14711.

(26) (a) Mino, H.; Kawamori, A. *Biochim. Biophys. Acta* **1994**, *1185*, 213−220. (b) Tang, X.-S.; Zheng, M.; Chisholm, D. A.; Dismukes, G. C.; Diner, B. A. *Biochemistry* **1996**, *35*, 1475−1484.

(27) (a) Tamura, N.; Cheniae, G. M. In *Light-Energy Transduction in Photosynthesis: Higher Plants and Bacterial Models*; Stevens, S. E., Jr., Stevens, Bryant, D. A., Eds.; The American Society of Plant Physiologists, 1988; pp 227−242. (b) Hoganson, C. W.; Ghanotakis, D. F.; Babcock, G. T.; Yocum, C. F. *Photosynth. Res.* **1989**, *22*, 285−293. (c) Miller, A.-F.; Brudvig, G. W. *Biochemistry* **1989**, *28*, 8181−8190. (d) Ananyev, G. M.; Dismukes, G. C. *Biochemistry* **1996**, *35*, 14608−14617.

insight into the structure and bulk accessibility of the $(Mn)_4Y_Z$ site and into the hydrogen-bonding status of the tyrosine. Characterization of $Y_Z^\bullet$ in native PSII, however, is hampered by the fast kinetics of the system; Y_Z is oxidized by P_{680}^+ on the nanosecond time scale[28] and rereduced by the $(Mn)_4$ cluster within 10's of μs to 1 ms,[3,29] which prevents the buildup of a high steady-state concentration of $Y_Z^\bullet$ under conditions when water is the substrate. Upon removal of the $(Mn)_4$ cluster,[30] or of Ca^{2+}, the rereduction of $Y_Z^\bullet$ is slowed, which allows cryotrapping of the radical.[26,33,34] In Mn-depleted PSII, Y_Z is oxidized by P_{680}^+ within 10's of μs,[35] and is rereduced on the order of 10's to 100's of ms.[36,37] In Ca-depleted samples, Y_Z is oxidized by P_{680}^+ on the microsecond time scale,[38] and the enzyme is blocked upon formation of $S_2Y_Z^\bullet$.[14,23,24] The regeneration of S_2Y_Z is slow and occurs on the seconds time scale.[39]

In the work presented here, we have cryotrapped $Y_Z^\bullet$ and $S_2Y_Z^\bullet$ in samples depleted of Mn, Ca^{2+}, and Cl^- and in samples exclusively devoid of Ca^{2+}, respectively. The paramagnetic species were studied by ESEEM spectroscopy to derive quantitative information on $^1H\backslash^2H$-exchangeable nuclei in the Y_Z site from these two types of PSII preparations. Analysis of the ESEEM data provides information of the number of exchangeable protons in the $Y_Z^\bullet$ site, their hyperfine couplings, and how these properties change as a function of the cofactor composition of the metal site.[40] We consider the implications of these results for several PSII phenomena including proton release, photoactivation, and redox-induced chlorophyll bandshifts, and end by discussing these data within the framework of the proposed metalloradical models for the water-splitting process.

Materials and Methods

Sample Preparations. PSII-enriched BBY membranes were prepared from market spinach according to the method developed by Yocum and co-workers, with 1 mM of EDTA included in all steps of the preparation.[42,43] The final resuspension buffer (SMN buffer) contained 0.4 M sucrose, 40 mM MES pH 6.5, and 20 mM NaCl. BBY samples at a final concentration of 0.5 mg of Chl/mL were depleted of manganese by incubation in 0.8 M TRIS buffer, pH 8.0 at 23 °C and containing 1.0 mM EDTA, at 0 °C for 20 min in room light. The Mn-depleted BBYs were collected by centrifugation, washed once in 40 mM MES pH 6.5, 20 mM NaCl, and 1.0 mM EDTA, and finally resuspended in 25% v/v glycerol, 40 mM MES pH 6.5, 20 mM NaCl, and 1.0 mM EDTA. Calcium-depleted PSII samples containing the three extrinsic polypeptides were prepared by the low-pH method,[44] and samples lacking the 17 and 23 kDa extrinsic subunits were generated by using the NaCl/EDTA procedure.[45] The samples devoid of Ca^{2+} were resuspended in SMN buffer containing 1.0 mM EDTA. The presence of the 17, 23, and 33 kDa subunits in the low-pH treated samples was verified with SDS-PAGE (not shown). The sucrose (BDH ARISTAR) used for the Ca-depletion procedures contained $\leq$1 ppm of Ca^{2+}. The samples were frozen in liquid N_2 and stored at −80 °C until use.

Oxygen Evolution. The oxygen-evolving activities of the PSII preparations were measured at 25 °C in a Clark-type oxygen electrode at a Chl concentration of 6.7 μg/mL in SMN buffer at pH 6.0. 2,6-Dichlorobenzoquinone at a final concentration of 0.5 mM was used as the external electron acceptor. The oxygen-evolving rates were typically 800 μmol O_2/mg of Chl*h in native samples, 0 upon Mn depletion, and <100 and 600 upon Ca depletion and Ca repletion, respectively. The oxygen-evolving activity in the low-pH treated, Ca-repleted samples was found to be unaffected by incubation in ^2H_2O buffer, as compared to incubation in ^1H_2O buffer, even after more than 2 h of incubation.

$^1H\backslash^2H$-Isotope Exchange Procedures. For $^1H\backslash^2H$-isotope exchange, the Mn-depleted samples were washed three times in ^2H_2O buffer containing 25% v/v glycerol, 40 mM MES pD 6.5 (pD = pH + 0.4), 20 mM NaCl, and 1.0 mM EDTA, and resuspended in 25% fully deuterated glycerol, 40 mM MES pD 6.5, 20 mM NaCl, and 1 mM EDTA. The samples devoid of calcium were washed three times and finally resuspended in ^2H_2O buffer containing 0.4 M sucrose (BDH ARISTAR), 40 mM MES pD 6.5, 20 mM NaCl, and 1 mM EDTA. The isotope exchange was performed on ice in weak room light. The ^1H contamination after the $^1H\backslash^2H$-isotope exchange was estimated to <8%. The $^1H\backslash^2H$ procedure was done immediately prior the cryotrapping procedures.

Low-Temperature Trapping Procedures. For the Mn-depleted samples, phenyl-*p*-benzoquinone (PPBQ) and $K_3Fe(CN)_6$ were used as electron acceptors at final concentrations of 2.5 and 20 times the concentration of PSII centers, respectively. For the Ca-depleted system, PPBQ was used at a final concentration of 10 times the PSII concentration, which was typically 27 μM (6.0 ± 0.2 mg Chl/mL) in the samples prepared for the cryotrapping procedure. After the addition of the electron acceptors, the samples were transferred into calibrated EPR tubes, 4.0 mm OD, and placed in a glass dewar positioned between two 410 W/82 V lamps (Osram Sylvania Inc., Winchester, KY) on an optical bench equipped with a light-collection system. The two lamps were connected to variable voltage transformers and the light intensity at the samples was about 30 mE m^2 s^{-1} per lamp. The Mn-depleted samples were illuminated for 5 s at 0 ± 1 °C, followed by illumination for 10 s as the temperature of the samples was lowered in an ethanol/solid CO_2/liquid N_2 bath maintained at − 90 °C. The light was then switched off and the samples were rapidly transferred to liquid N_2 and then directly to the EPR spectrometer. The same procedure was performed for the Ca-depleted samples with the exception that these samples were illuminated for 10 s at 0 ± 1 °C, followed by illumination

(28) (a) Brettel, K.; Schlodder, E.; Witt, H. T. *Biochim. Biophys. Acta* **1984**, *766*, 403−415. (b) Meyer, B.; Schlodder, E.; Dekker: J. P.; Witt, H. T. *Biochim. Biophys. Acta* **1989**, *974*, 36−43.

(29) Razeghifard, M. R.; Klughammer, C.; Pace, R. J. *Biochemistry* **1997**, *36*, 86−92.

(30) With respect to the presence of the Ca^{2+} and Cl^- cofactors upon Mn depletion, this procedure is most likely equivalent to Mn/Ca/Cl depletion since there is a drastic decrease in both Ca^{2+} and Cl^- affinity in Mn-depleted samples.[27a, 31, 32]

(31) Ädelroth, P.; Lindberg, K.; Andréasson, L.-E. *Biochemistry* **1995**, *34*, 9021−9027.

(32) Lindberg, K.; Vänngård, T.; Andréasson, L.-E. *Photosynth. Res.* **1993**, *38*, 401−408.

(33) (a) Boussac, A.; Zimmermann, J.-L.; Rutherford, A. W. *Biochemistry* **1989**, *28*, 8984−8989. (b) Sivaraja, M.; Tso, J.; Dismukes, G. C. *Biochemistry* **1989**, *28*, 9459−9464.

(34) Kodera, Y.; Takura, K.; Mino, H.; Kawamori, A. In *Research in Photosynthesis*; Murata, N., Ed.; Kluwer Academic Publishers: The Netherlands, 1992; Vol. II, pp 57−60.

(35) Conjeaud, H.; Mathis, P. *Biochim. Biophys. Acta* **1980**, *590*, 353−359.

(36) Babcock, G. T.; Sauer, K. *Biochim. Biophys. Acta* **1975**, *376*, 329−344.

(37) Yerkes, C. T.; Babcock, G. T. *Biochim. Biophys. Acta* **1980**, *590*, 360−372.

(38) Boussac, A.; Sétif, P.; Rutherford, A. W. *Biochemistry* **1992**, *31*, 1224−1234.

(39) (a) Ghanotakis, D. F.; Babcock, G. T.; Yocum, C. F. *Biochim. Biophys. Acta* **1984**, *765*, 388−398. (b) Andréasson, L.-E.; Vass, I.; Styring, S. *Biochim. Biophys. Acta* **1995**, *1230*, 155−164. (c) Boussac, A.; Rutherford, A. W. *Biochim. Biophys. Acta* **1995**, *1230*, 195−201. (d) Lydakis-Simantiris, N.; Dorlet, P.; Ghanotakis, D. F.; Babcock, G. T. *Biochemistry* **1998**, *37*, 6427−6435; Errata, *Biochemistry* **1998**, *37*, 8816−8816.

(40) Preliminary analyses of these results have been presented in refs 20c and 41.

(41) Babcock, G. T.; Espe, M.; Hoganson, C.; Lydakis-Simantiris, N.; McCracken, J.; Shi, W.; Styring, S.; Tommos, C.; Warncke, K. *Acta Chem. Scand.* **1997**, *51*, 533−540.

(42) Berthold, D. A.; Babcock, G. T.; Yocum, C. F. *FEBS Lett.* **1981**, *134*, 231−234.

(43) Ghanotakis, D. F.; Topper, J. N.; Babcock, G. T.; Yocum, C. F. *FEBS Lett.* **1984**, *170*, 169−173.

(44) Ono, T.; Inoue, Y. *FEBS Lett.* **1988**, *227*, 147−152.

(45) Ono, T.; Inoue, Y. *Biochim. Biophys. Acta* **1990**, *1020*, 269−277.

for 15 s as the temperature was lowered to −90 °C. The temperature in the samples during the illumination was controlled by a flowing N_2-gas system, cooled by a 200 K ethanol/solid CO_2 bath, connected to the glass dewar. For induction and trapping of $Y_D^\bullet$, the Mn-depleted samples were illuminated for 5−10 s at 0 ± 1 °C and then frozen in the dark.

EMR Spectroscopies. Continuous-wave EPR measurements were made on a Bruker ESP 300E X-band spectrometer equipped with an TE_{102}-mode cavity. Measurements at 77 K were performed by using a liquid N_2 finger dewar. For measurements below 77 K, the spectrometer was equipped with a liquid He cryostat and temperature controller from Oxford Instruments. Processing of the cw-EPR spectra was performed by using the ESP 300E software. The ESEEM spectra were recorded by using a pulsed EPR spectrometer constructed at Michigan State University.[46] Processing of the experimental data, Fourier transform, and simulation of powder-pattern ESEEM[47] were performed by using the Matlab program provided by Matworks Inc. (Natick, MA). Dead-time reconstruction of the experimental and simulated time-domain data was calculated as described.[48]

Results

Cryotrapping of $Y_Z^\bullet$ in Cofactor-Depleted PSII. To study the Y_Z site by ESEEM at different levels of disintegration of the OEC, procedures were developed for trapping the transient $Y_Z^\bullet$ and $S_2Y_Z^\bullet$ states at high yield in Mn-depleted and in Ca-depleted PSII samples, respectively. About 70% of $Y_Z^\bullet$ could be trapped at low temperature in Mn-depleted BBY samples, as shown in Figure 1A. The dark trace, spectrum b, represents the stable $Y_D^\bullet$ radical, and the light-induced increase observed in spectrum a represents cryotrapped $Y_Z^\bullet$. The pure $Y_Z^\bullet$ spectrum is shown as the light-minus-annealed trace in spectrum c. Small differences in line width and hyperfine structure are observed between the $Y_Z^\bullet$ and $Y_D^\bullet$ spectra shown in Figure 1A, which are consistent with earlier studies.[12,26] The $Y_Z^\bullet$ spectrum is slightly more resolved and has a peak-to-trough line width of about 22 G, as compared to the line width of the $Y_D^\bullet$ spectrum, which is 20 G in spinach. The hyperfine interactions to the tyrosine ring- and β-methylene protons and the electron spin-density distribution of $Y_Z^\bullet$ and $Y_D^\bullet$, which are reflected in their overall cw-EPR line shapes, have been evaluated in detail.[12,13d,49,50]

Figure 1B shows 4900 G wide cw-EPR spectra obtained from Ca-depleted samples, in the absence and presence of the 17 and 23 kDa extrinsic polypeptides. The two top spectra in Figure 1B represent a NaCl/EDTA-washed BBY sample frozen during illumination (black spectrum) and after a 10 min dark incubation at 0 °C (gray spectrum). The 145 G wide, light-induced signal centered in the $g = 2$ region is apparent in the sample frozen during illumination and represents the magnetically coupled $S_2Y_Z^\bullet$ state in Ca-depleted PSII.[23,51] The two bottom spectra in Figure 1B represent a low-pH treated BBY sample frozen during illumination (black spectrum) and prior to illumination (gray spectrum). In the low-pH treated samples, which contain all three extrinsic polypeptides, the $S_2Y_Z^\bullet$ signal is 190 G peak-to-trough. In addition to $S_2Y_Z^\bullet$, there are several paramagnetic

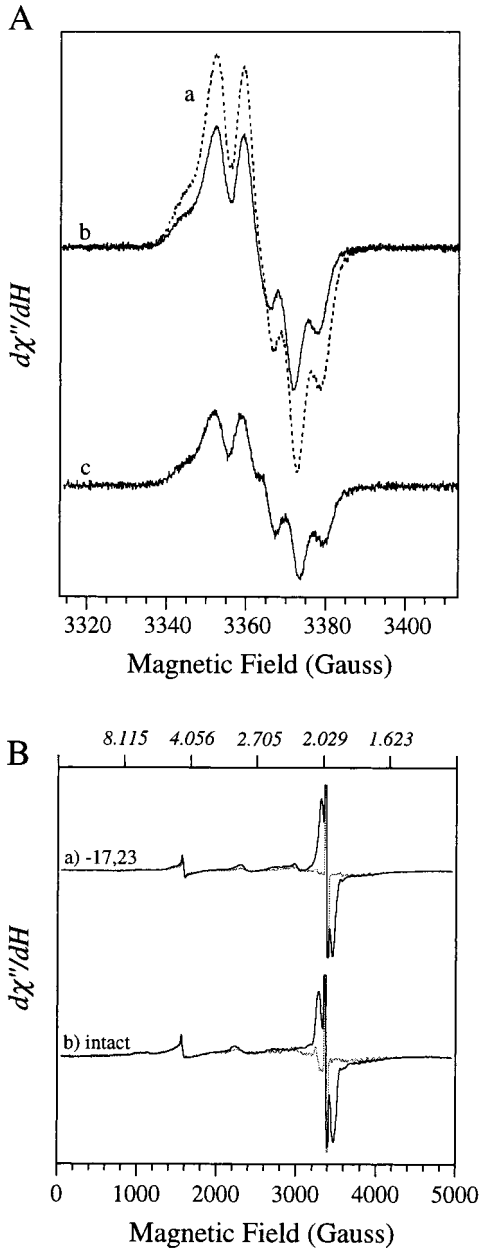

Figure 1. (A) Continuous-wave EPR spectra obtained at 77 K on a Mn-depleted, PSII-enriched BBY sample from spinach (a) frozen during illumination, (b) after two min at 20 °C in the dark, and (c) light-minus-annealed difference spectrum. The spectra were obtained with nonsaturating microwave power. Experimental conditions: ν_{mw} 9.433 GHz; power 9.2 μW; modulation amplitude 1.6 G; time constant 41 ms; scan rate 0.6 G/s; 20 scans/spectrum; [Chl] 8.3 ± 0.2 mg/mL; temperature 77 K. (B) Continuous-wave EPR spectra of Ca-depleted BBY membranes in the absence and presence of the 17 and 23 kDa extrinsic polypeptides. (a) Spectra representing a NaCl/EDTA-washed sample frozen during illumination (black spectrum) and after 10 min at 0 °C in the dark (gray spectrum). (b) Spectra obtained on an intact, low-pH treated BBY sample frozen during illumination (black spectrum) and prior to the illumination (gray spectrum). Experimental conditions: ν_{mw} 9.464 GHz; power 7.9 mW; modulation amplitude 20.1 G; time constant 82 ms; scan rate 14.6 G/s; 1 scan/spectrum; [Chl] 6.0 ± 0.2 mg/mL; temperature 10 K.

(46) McCracken, J.; Shin, D.-H.; Dye, J. L. *Appl. Magn. Reson.* **1992**, *3*, 305−316.

(47) (a) Mims, W. B. *Phys. Rev. B* **1972**, *5*, 2409−2419. (b) Mims, W. B. *Phys. Rev. B* **1972**, *6*, 3543−3545.

(48) Mims, W. B. *J. Magn. Reson.* **1984**, *59*, 291−306.

(49) (a) Hoganson, C. W.; Babcock, G. T. *Biochemistry* **1992**, *31*, 11874−11880. (b) Rigby, S. E. J.; Nugent, J. H. A.; O'Malley, P. J. *Biochemistry* **1994**, *33*, 1734−1742. (c) Tommos, C.; Madsen, C.; Styring, S.; Vermaas, W. *Biochemistry* **1994**, *33*, 11805−11813

(50) (a) Hoganson, C. W.; Sahlin, M.; Sjöberg, B.-M.; Babcock, G. T. *J. Am. Chem. Soc.* **1996**, *118*, 4672−4679. (b) Dole, F.; Diner, B. A.; Hoganson, C. W.; Babcock, G. T.; Britt, R. D. *J. Am. Chem. Soc.* **1997**, *119*, 11540−11541.

(51) The $S_2Y_Z^\bullet$ state forms a tyrosyl−manganese exchange-coupled system, whose EPR spectrum contains the prominent, split features in the $g = 2$ region dominated by $Y_Z^\bullet$ transitions and the low intensity, ∼2000 G wide multiline part dominated by $(Mn)_4$ transitions (for a discussion, see refs 23b and 23c). The "$S_2Y_Z^\bullet$" notation used here refers to the split, $g = 2$ region of the whole spectrum.

centers that are routinely detected in PSII samples.[52] The spectrum from $Y_D^{\bullet}$ occurs as the narrow feature centered at 3372 G. A feature assigned to rhombic Fe^{3+} is observed at $g = 4.3$. The g_y and g_z components of the low-spin heme from cytochrome b_{559} are observed at $g \approx 2.3$ and 3.0, respectively.[53] In some preparations, we observed a feature at $g = 2.067$, which we assign to Cu^{2+}.[54] In Ca-depleted samples prepared with millimolar concentrations of chelators, the S_2 multiline signal[55] exhibits a modified, less-resolved spectrum, which, once induced, remains stable for several hours in the dark.[33,45,56] Spin-quantifications on the $S_2Y_Z^{\bullet}$ signal obtained from the two Ca-depleted preparations indicate that we can trap ~75% of the PSII center in the $S_2Y_Z^{\bullet}$ state (not shown).[57] We estimate the absolute spin concentrations to be about 27 and 20 μM for $Y_D^{\bullet}$ and $Y_Z^{\bullet}/S_2Y_Z^{\bullet}$, respectively.

Exchangeable ^{1}H Nuclei in the Y_Z Site. The ^{1}H\$^2$H exchange rate and the hyperfine (hf) interactions of exchangeable protons in the Y_Z site in the two cofactor-depleted systems were studied by 2- and 3-pulse ESEEM spectroscopy. The different magnetic properties of the ^{1}H and ^{2}H nuclei combined with the ESEEM technique provide a sensitive tool to study the accessibility by the bulk phase to the Y_Z site. Upon complete ^{1}H\$^2$H exchange, the hf interactions with ^{2}H nuclei can be analyzed to derive information on the protein environment surrounding Y_Z. The hyperfine interaction between $Y_Z^{\bullet}$ and a nearby nuclear spin is given by $A = A_{iso} + A_{dip}$, where A_{iso} represents the isotropic Fermi contact interaction and A_{dip} is the anisotropic dipole−dipole coupling term.[58] For the weakly coupled nuclei studied here, we assume point-dipole interactions between the electron spin and the surrounding nuclear spins. This type of interaction is represented by axial hf tensors that contain the following elements:

$$A_{xx} = A_{yy} = A_{iso} - T_{dip} \text{ and } A_{zz} = A_{iso} + 2T_{dip} \quad (1)$$

$$T_{dip} = \rho g_e g_N \beta_e \beta_N r^{-3} \quad (2)$$

where ρ is the electron spin density on the atom to which the nucleus is coupled, g_e is the experimental electron g value, g_N is the nuclear g value, β_e and β_N are the Bohr and nuclear magneton, respectively, and r represents the radial distance between the two coupled spin centers. For a ^{2}H or a ^{1}H nucleus coupled to $Y_Z^{\bullet}$, with a g_e of 2.00466,[59] $T_{dip}(\text{MHz}) = \rho 12.15 r^{-3}$ (Å^3) and $T_{dip}(\text{MHz}) = \rho 79.16 r^{-3}$ (Å^3), respectively.

(a) Solvent Accessibility to the Y_Z Site. There are substantial differences in accessibility by the bulk medium to the Y_Z site as compared to Y_D, which are well demonstrated by ^{1}H\$^2$H-isotope exchange combined with ESEEM spectroscopy. The experimentally observed time-domain trace from a 2-pulse, 90°−τ−180° experiment, derived by plotting the integrated spin−echo intensity as a function of τ, is given by:[60−62]

$$E(\tau) = V_{decay} \prod_{i=1}^{N} E^i_{mod}(\tau) \quad (3)$$

where V_{decay} describes the decay of the overall echo intensity due to spin-relaxation mechanisms, N represents the number of nuclei magnetically coupled to the electronic spin, and for a $S = {}^1/_2$ and $I = {}^1/_2$ system:[63,64]

$$E_{mod}(\tau) = 1 - k/2 + k/2[\cos(2\pi\nu_\alpha\tau) + \cos(2\pi\nu_\beta\tau)] - k/4[\cos(2\pi(\nu_\alpha + \nu_\beta)\tau) + \cos(2\pi(\nu_\alpha - \nu_\beta)\tau)] \quad (4)$$

The ν_α and ν_β are the frequency components representing the fundamental, $\Delta m_I = \pm 1$ hf transitions associated with the $+{}^1/_2$ and $-{}^1/_2$ spin manifolds, respectively. The k factor is defined as the modulation depth parameter and is given by:[65]

$$k = (\nu_I B/\nu_\alpha\nu_\beta)^2 \quad (5)$$

The ν_I term is the Larmor frequency of the coupled nucleus, and $B = 3T_{dip}(\cos\theta \sin\theta)$ where θ represents the angle between the external magnetic field and the line joining the electron and nuclear spins.

Figure 2 displays 2-pulse ESEEM data from $Y_D^{\bullet}$ in Mn-depleted samples after 35 min (trace a), 75 min (trace b), 24 h (trace c), and 46 h (trace d) of ^2H_2O incubation. The poor accessibility by solvent water to the Y_D site is revealed by the long ^2H_2O incubation required to reduce the appearance of ^{1}H modulations in the $Y_D^{\bullet}$ ESEEM pattern. In Figure 2, the fundamental ($\nu_{\alpha,\beta}$) and sum-combination ($\nu_\alpha + \nu_\beta$) hf frequencies of the ^{1}H nuclei coupled to $Y_D^{\bullet}$ are seen as the rapid modulation with periods of 37 and 73 ns, respectively. Concomitant with the decrease of the ^{1}H modulations, the fundamental ^{2}H modulation with a period of 478 ns appears in the spin−echo envelope. These results show that ^{1}H\$^2$H exchange at the Y_D site occurs on the hour time scale, consistent with earlier work.[67]

In contrast, for the Y_Z site in Ca-depleted PSII the ^{1}H\$^2$H exchange is completed with an upper limit on the minute time scale, as shown by the 3-pulse ESEEM data displayed in Figures

(52) Miller, A.-F.; Brudvig, G. W. *Biochim. Biophys. Acta* **1991**, *1056*, 1−18.

(53) Babcock, G. T.; Widger, W. R.; Cramer, W. A.; Oertling, W. A.; Metz, J. G. *Biochemistry* **1985**, *24*, 3638−3645.

(54) Sheptovitsky, Y. G.; Brudvig, G. W. *Biochemistry* **1996**, *35*, 16255−16263.

(55) Dismukes, G. C.; Siderer, Y. *FEBS Lett.* **1980**, *121*, 78−80.

(56) Boussac, A.; Zimmermann, J.-L.; Rutherford, A. W. *FEBS Lett.* **1990**, *277*, 69−74.

(57) Due to the exchange-coupled nature of the $S_2Y_Z^{\bullet}$ state, the area of the light-minus-annealed $S_2Y_Z^{\bullet}$ signal in the $g = 2$ region may exceed one spin per PSII, when compared to the area of $Y_D^{\bullet}$, which was used as the spin standard. If this is the case, the 75% estimate represents an upper limit in the $S_2Y_Z^{\bullet}$ trapping yield.

(58) (a) Gordy, W. In *Techniques of Chemistry Vol. XV: Theory and Applications of Electron Spin Resonance;* West, W., Ed.; John Wiley & Sons: New York, 1980. (b) Atherton, N. M. *Principles of Electron Spin Resonance;* Ellis Horwood and PTR Prentice Hall: London, 1993. (c) Weil, J. A.; Bolton, J. R.; Wertz, J. E. *Electron Paramagnetic Resonance: Elementary Theory and Practical Applications;* John Wiley & Sons: New York, 1994. (d) Piekara-Sady, L.; Kispert, L. D. In *Handbook of Electron Spin Resonance: Data Sources, Computer Technology, Relaxation, and ENDOR.;* Poole, C. P., Jr., Farach, Eds.; H. A., AIP Press: New York, 1994; pp 311−357.

(59) Un, S.; Tang, X.-S.; Diner, B. A. *Biochemistry* **1996**, *35*, 679−684.

(60) Rowan, L. G.; Hahn, E. L.; Mims, W. B. *Phys. Rev.* **1965**, *137*, A61-A71.

(61) (a) Kevan, L. In *Time Domain Electron Spin Resonance;* Kevan, L., Schwartz, R. N., Eds.; John Wiley & Sons: New York, 1979; pp 279−341. (b) *ESEEM Spectroscopy;* Dikanov, S. A., Tsvetkov, Y. D., Eds.; CRC Press: Ann Arbor, 1994.

(62) (a) Mims, W. B.; Peisach, J. In *Advanced EPR: Applications in Biology and Biochemistry;* Hoff, A. J., Ed.; Elsevier: New York, 1989; pp 1−57. (b) McCracken, J. In *Handbook of Electron Spin Resonance*; Poole, C. P., Jr., H. A., Farach, Eds.; Vol. II, in press.

(63) The $S_2Y_Z^{\bullet}$ state is an exchange-coupled system, but appears to be in the weak-coupling limit.[23b,c] Within this assumption, we analyze the deuterium ESEEM data obtained on $S_2Y_Z^{\bullet}$ from the Ca-depleted samples in a $S = {}^1/_2$, $I = 1$ context, rather than with a $S = 1$, $I = 1$ spin model.

(64) The 2- and 3-pulse modulation functions for a $S = {}^1/_2$ and $I = 1$ system contain, in addition to the terms shown in eqs 4 and 7, higher order terms with respect to k and components arising from nuclear quadrupole interactions (see ref 61, and references therein).

(65) For the spin = 1 ^{2}H nucleus, k is equal to $8/3(\nu_I B/\nu_\alpha\nu_\beta)^2$.

(66) (a) Babcock, G. T.; Sauer, K. *Biochim. Biophys. Acta* **1973**, *325*, 504−519. (b) Ghanotakis, D. F.; Yerkes, C. T.; Babcock, G. T. *Biochim. Biophys. Acta* **1982**, *682*, 21−31.

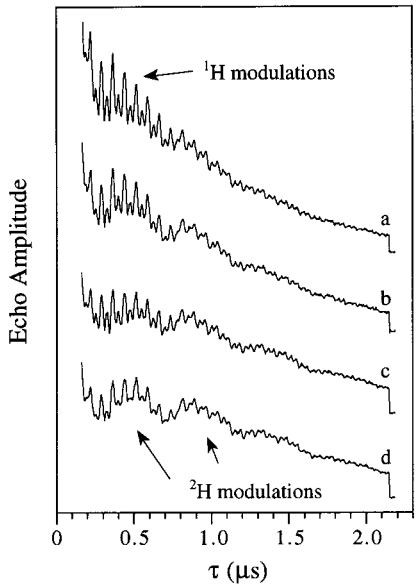

Figure 2. Two-pulse ESEEM obtained on $Y_D^\bullet$ in Mn-depleted BBYs incubated in ^2H_2O for (a) 35 min, (b) 75 min, (c) 24 h, and (d) 46 h. The traces shown represent light-minus-reduced difference data. The background traces were obtained by adding 0.2 mM carbonylcyanide-*m*-chlorophenylhydrazone to the thawed samples, incubate in the dark for 10 min at 20 °C to reduce $Y_D^\bullet$.[66] The samples were then refrozen in the dark. The ESEEM traces shown were obtained at the center field of the $Y_D^\bullet$ EPR spectrum. The baseline in the time-domain traces is derived by displacing the integrator away from the electron spin−echo for the last 10 points of the acquisition. Experimental conditions: ν_{mw} (a, b) 8.990 and (c, d) 8.960 GHz; H_0 (a, b) 3204 and (c, d) 3194 G; starting τ 140 ns; microwave pulse power 40−50 W; pulse sequence repetition rate 20 Hz; events per point 10; each scan contains 512 points collected at 4 ns increments; 6 scans/trace; [Chl] 6.0 ± 0.2 mg/mL; temperature 4.2 K.

3 and 4. In a 3-pulse, 90°−τ−90°−T−90° spin−echo experiment the intensity of the stimulated echo, which appears at a time equal to τ after the third microwave pulse, is plotted as a function of T. The observed spin−echo envelope for a $S = {}^1/_2$ and $I = {}^1/_2$ spin interaction is described by:[61−65,68]

$$E(\tau,T) = V_{\text{decay}} \frac{1}{2}[\prod_{i=1}^{N} E^i_\alpha(\tau,T) + \prod_{j=1}^{N} E^j_\beta(\tau,T)] \qquad (6)$$

$$E_{\alpha,\beta}(\tau,T) = 1 - k/2[(\sin^2(\pi\nu_\alpha\tau))(1 - \cos(2\pi\nu_\beta(\tau + T))) + (\sin^2(\pi\nu_\beta\tau))(1 - \cos(2\pi\nu_\alpha(\tau + T)))] \quad (7)$$

Figure 3 shows 3-pulse ESEEM representing $S_2Y_Z^\bullet$ in low-pH treated, Ca-depleted BBY samples after ^2H_2O incubation for 40 min (trace a) and for 60 min (trace b). As opposed to the $Y_D^\bullet$ data in Figure 2, in which the deuterium modulations continuously grow into the ESEEM pattern as the ^2H_2O incubation period is increased, the two sets of data obtained on $S_2Y_Z^\bullet$ are, within the signal-to-noise, identical. Figure 4 shows the corresponding frequency-domain spectra obtained by Fourier transform of the time-domain data in Figure 3. The depth of the ^2H modulation is the same in the two traces shown in Figure

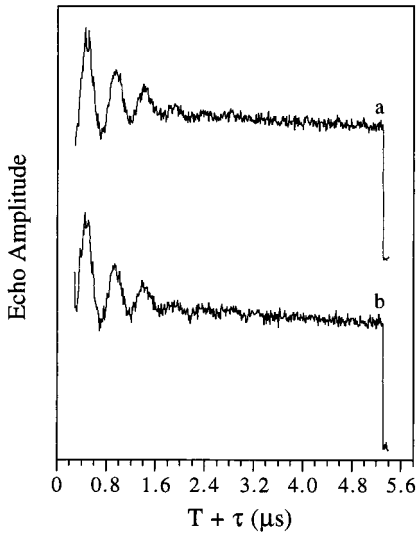

Figure 3. Three-pulse ESEEM recorded on $S_2Y_Z^\bullet$ in Ca-depleted BBYs incubated in ^2H_2O for (a) 40 and (b) 60 min. The time-domain traces shown represent light-minus-dark difference data. The difference data were obtained by dividing each sample, after $^1H\backslash^2H$ exchange and addition of PPBQ, into two calibrated EPR tubes. One sample was frozen during illumination and the other in the dark. The $S_2Y_Z^\bullet$ ESEEM data shown were obtained 40 G upfield from the center field of the $Y_D^\bullet$ spectrum, and are reproducible at other field positions within the $S_2Y_Z^\bullet$ EPR spectrum (not shown). Experimental conditions: ν_{mw} (a) 8.990 and (b) 8.980 GHz; H_0 (a) 3248 and (b) 3244 G; τ (a) 238 and (b) 236 ns; starting T (a) 42 and (b) 44 ns; microwave pulse power 40−50 W; pulse sequence repetition rate 60 Hz; events per point 32; each scan contains 512 points collected at 10 ns increments; 20 scans/trace; [Chl] 6.0 ± 0.2 mg/mL; temperature 1.8 K.

3, which is reflected in the frequency domain in that the amplitude of the fundamental ^2H peak, resonating at 2.11 MHz, from the two different samples is of equal height. The identical damping pattern of the two ESEEM traces in Figure 3 is reflected in the equal width of the ^2H peak, 0.48 MHz, in the two spectra in Figure 4. Two-pulse ESEEM obtained on $S_2Y_Z^\bullet$ gave results consistent with the 3-pulse data (not shown). Consequently, the $^1H\backslash^2H$ exchange at the Y_Z site in the Ca-depleted system is completed with 40 min representing the upper limit.

A similar set of data were obtained for $Y_Z^\bullet$ in the Mn-depleted system. For these samples the $^1H\backslash^2H$ exchange at the Y_Z site was completed within 35 min (not shown).

(b) ESEEM Analysis. Figure 5 displays a comparison of the $S_2Y_Z^\bullet$ ESEEM pattern from Ca-depleted PSII after complete $^1H\backslash^2H$ exchange, and simulated data based on a $S = {}^1/_2$, $I = 1$ model in which the number of magnetically coupled nuclei and the magnitude of the hf interactions were varied.[63] In Figure 5A two calculated ESEEM traces are shown: trace a was simulated with a weak hf interaction to one deuteron with T_{dip} equal to 0.22 MHz (^1H 1.43 MHz); trace b was calculated with a T_{dip} of 0.54 MHz (^1H 3.52 MHz), which corresponds to the hf coupling measured for the hydrogen bond of $Y_D^\bullet$.[67,69] The simulated data in Figures 5B represent the same strength in the hf couplings, T_{dip} equal to 0.22 (trace a) and 0.54 MHz (trace b), respectively, but include two interacting deuterons. Other parameters used to generate the simulated ESEEM traces are given in the caption to Figure 5.

The calculated time-domain data in Figure 5 show the sensitivity of the ESE modulation pattern to changes in the

(67) (a) Rodriguez, I. D.; Chandrashekar, T. K.; Babcock, G. T. In *Progress in Photosynthesis Research*; Biggins, J., Ed.; Martinus Nijhoff Publishers: The Netherlands, 1987; Vol. I, pp 471−474. (b) Tang, X.-S.; Chisholm, D. A.; Dismukes, G. C.; Brudvig, G. W.; Diner, B. A. *Biochemistry* **1993**, *32*, 13742−13748.

(68) Dikanov, S. A.; Shubin, A. A.; Parmon, V. N. *J. Magn. Reson.* **1981**, *42*, 474−487.

(69) Force, D. A.; Randall, D. W.; Britt, R. D.; Tang, X.-S.; Diner, B. A. *J. Am. Chem. Soc.* **1995**, *117*, 12643−12644.

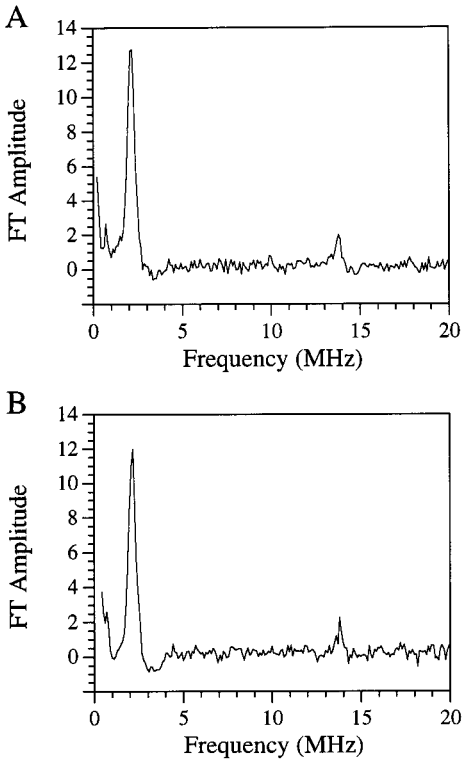

Figure 4. (A) Frequency-domain spectrum obtained by Fourier transform of the $S_2Y_Z^\bullet$ time-domain trace a in Figure 3, and (B) corresponding frequency-domain spectrum of trace b in Figure 3. The features resonating at 2.11 and 13.7 MHz correspond to the fundamental hf frequencies of the incorporated ^{2}H and nonexchangeable ^{1}H nuclei coupled to $S_2Y_Z^\bullet$, respectively.

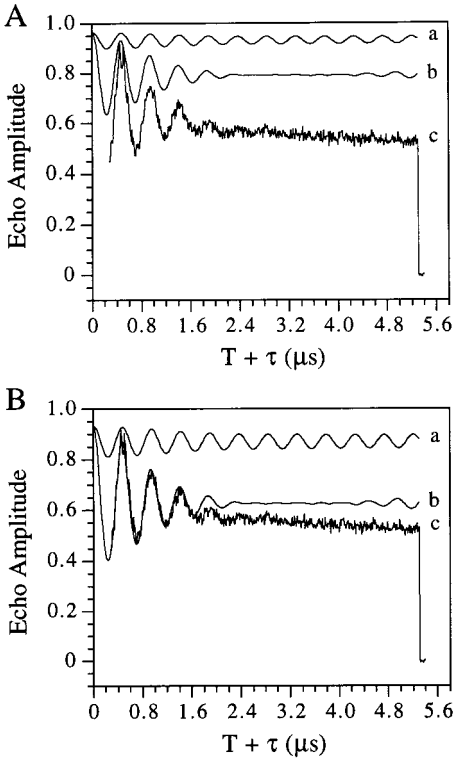

Figure 5. Three-pulse ESEEM representing $S_2Y_Z^\bullet$ in Ca-depleted PSII compared to simulations. The $S_2Y_Z^\bullet$ time-domain data (trace c) are the same as shown in Figure 3 trace a. The calculated ESEEM traces represent (A) one ^{2}H nucleus with T_{dip} equal to (a) 0.22 and (b) 0.54 MHz and (B) two ^{2}H nuclei with a T_{dip} of (a) 0.22 and (b) 0.54 MHz. Simulation parameters: H_0 3248 G; τ 238 ns; A_{iso} 0 MHz; e^2qQ 0.25 MHz; η 0.

magnetic environment of the unpaired electron spin. The frequency of the modulation depends on the identity of the coupled nucleus and on the strength of the electron−nuclear interaction. The depth of the modulation with respect to the overall echo height is sensitive to the anisotropy of the hf interactions and to the number of nuclei involved. The damping of the modulation pattern becomes considerably more pronounced as the dipole−dipole interaction increases. The ESEEM pattern of weakly coupled deuterons will also be influenced by nuclear quadruple couplings, albeit these effects are substantially smaller relative to the hf interactions.[61]

The time-domain data recorded on $S_2Y_Z^\bullet$ in Ca-depleted PSII exhibit fairly deep, rapidly damping ^{2}H modulations. From a direct comparison between the $S_2Y_Z^\bullet$ trace and the simulated data sets in Figure 5, two conclusions can be made. First, the overall fit to the modulation pattern is better with T_{dip} on the order of 0.54 MHz; the shallow modulations representing the weak, 0.22 MHz interaction do not provide a good fit. Second, the ESE modulation depth cannot be reproduced by a single deuteron. ESEEM traces calculated for one ^{2}H with $T_{dip} > 0.54$ MHz exhibit dominant modulation damping and the overall ESEEM pattern deviates considerably from the $S_2Y_Z^\bullet$ trace (not shown). Trace b in Figure 5B, which includes 2 deuterons with an average T_{dip} of 0.54 MHz, shows a fairly good fit to the $S_2Y_Z^\bullet$ trace.

From the coarse comparison between the calculated and experimental ESEEM data presented in Figure 5, we can conclude that there is more than one ^{2}H nucleus in the ^{1}H\$^2$H exchanged Y_Z site in Ca-depleted PSII. In addition, the depth and the damping of the ^{2}H modulations suggests hf interactions on the order of a moderately strong hydrogen bond.

In an ESEEM experiment, the observed modulation pattern will, in addition to the number of nuclei involved and the magnitude of the hf couplings, be effected by V_{decay}, the overall decay of the echo intensity due to relaxation processes (see above).[62b] A more detailed simulation analysis of the $S_2Y_Z^\bullet$ ESEEM data that includes spin relaxation is shown in Figure 6, parts A and B, which display two $S_2Y_Z^\bullet$ traces, obtained from two different preparations and recorded with different τ values. The experimental traces are overlaid with simulated data obtained with one set of hyperfine and quadrupole couplings (see caption for details). The calculated traces represent 2 deuterons with an average T_{dip} of 0.48 MHz (^{1}H 3.13 MHz). The frequency-domain spectra representing the experimental and simulated ESEEM traces in Figure 6A are shown in Figure 7A. The close fit of the depth and the damping of the $S_2Y_Z^\bullet$ trace is reflected in the good agreement between the experimental and calculated frequency-domain spectra. Figure 8 displays a 2-pulse trace calculated with 2 deuterons with T_{dip} equal to 0.48 MHz on top of a $S_2Y_Z^\bullet$ trace, which shows that the simulations are consistent with both 2- and 3-pulse data.

In the simulations, the 0.48 MHz value of T_{dip} represents an average of two interacting ^{2}H nuclei. A set of simulations were done to determine what the limits of this 0.48 MHz average are and if the fit could be improved by separating the hf values for the 2 interacting deuterons. The changes in the simulated data were within the noise of the experimental data to a separation in T_{dip} of 0.44 and 0.52 MHz, respectively. The fit of the experimental data did not improve by invoking an inequivalence in the hf couplings (not shown).

A similar analysis was done for three ^{2}H nuclei in which the hyperfine and quadrupole couplings were optimized to fit the

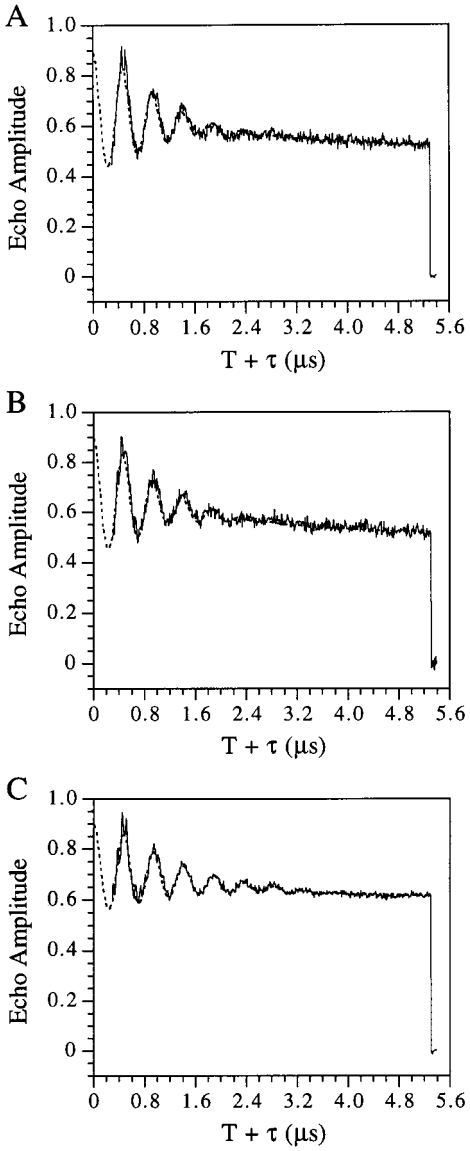

Figure 6. Experimental (solid lines) and simulated (dotted lines) 3-pulse ESEEM representing (A, B) $S_2Y_Z^\bullet$ in Ca-depleted PSII and (C) $Y_Z^\bullet$ in Mn-depleted samples. The experimental traces are (A, B) light-minus-dark and (C) light-minus-annealed difference data. Experimental conditions: ^2H_2O incubation (A) 40, (B) 60, and (C) 35 min; ν_{mw} (A) 8.990, (B) 8.980, and (C) 9.095 GHz; H_0 (A) 3248, (B) 3244, and (C) 3247 G; τ (A) 238, (B) 253, and (C) 235 ns; starting T (A) 42, (B) 37, and (C) 45 ns; microwave pulse power 40−50 W; pulse sequence repetition rate (A, B) 60 and (C) 20 Hz; events per point (A, B) 32 and (C) 10; each scan contains 512 points collected at 10 ns increments; (A, B) 20 scans/trace and (C) 6 scans/trace; [Chl] 6.0 ± 0.2 mg/mL; temperature (A, B) 1.8 and (C) 4.2 K. Simulation parameters: A_{iso} 0 MHz; e^2qQ 0.25 MHz; η 0; (A, B) two ^2H nuclei with T_{dip} equal to 0.48 MHz, (C) one ^2H nucleus with T_{dip} equal 0.40 MHz plus 3 deuterons with T_{dip} of 0.24 MHz. The H_0 and τ values for each simulated trace were identical to those for the corresponding experimental data. The V_{decay} function was simulated by $\exp(-(\tau + T)/t)^{1.5}$ with t equal to 2.6−2.8 μs.

experimental $S_2Y_Z^\bullet$ traces. A reasonably good fit could be obtained by assuming three ^2H nuclei with an average T_{dip} of 0.40 MHz (^1H 2.61 MHz). The fit of the 2- and 3-pulse experimental $S_2Y_Z^\bullet$ data, however, was clearly not as good as the fit with only 2 deuterons (not shown). We conclude that within an analysis based on a weak-coupling scenario for $S_2Y_Z^\bullet$, two exchangeable ^2H nuclei with $T_{dip} = 0.48 \pm 0.04$ MHz (^1H 3.13 ± 0.26 MHz) give the best fit of the experimental $S_2Y_Z^\bullet$ ESEEM data.

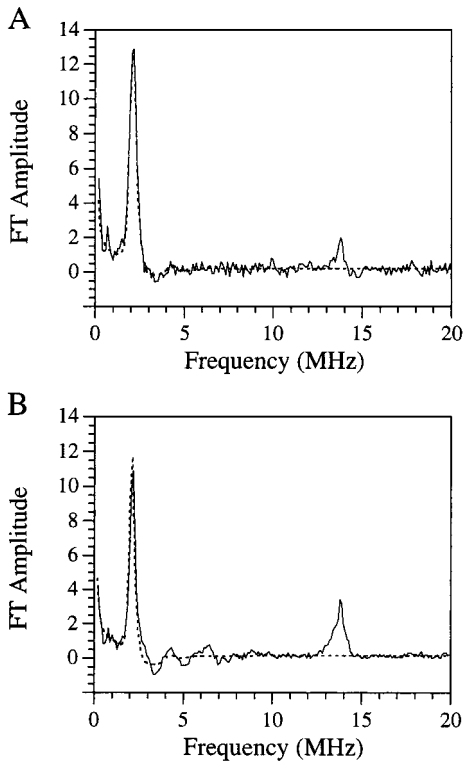

Figure 7. Frequency-domain spectra obtained by Fourier transform of the experimental and simulated (A) $S_2Y_Z^\bullet$ traces in Figure 6A and (B) $Y_Z^\bullet$ data in Figure 6C. A 280 ns deadtime, which is equal to the experimental value, was introduced into the simulated data prior to the Fourier transform.

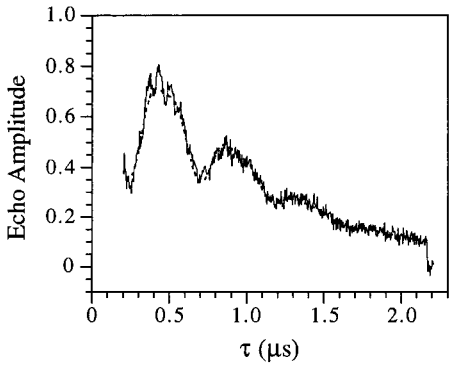

Figure 8. Experimental and simulated 2-pulse ESEEM representing $S_2Y_Z^\bullet$ in Ca-depleted samples. The experimental trace represents light-minus-dark difference data. Experimental conditions: ν_{mw} 8.990 GHz; H_0 3248 G; τ 160 ns; microwave pulse power 40−50 W; pulse sequence repetition rate 60 Hz; events per point 10; the scan contains 512 points collected at 4 ns increments; 10 scans/trace; [Chl] 6.0 ± 0.2 mg/mL; temperature 1.8 K. Simulation parameters: H_0 3248 G; τ 160; A_{iso} 0 MHz; e^2qQ 0.25 MHz; η 0; two ^2H nuclei with T_{dip} equal to 0.48 MHz. The V_{decay} function was simulated by $\exp(-\tau/1.2\mu s)^2$.

The same type of analysis as described above for $S_2Y_Z^\bullet$ in Ca-depleted PSII was performed on $Y_Z^\bullet$ in Mn-depleted samples. Figure 9 shows a 3-pulse $Y_Z^\bullet$ ESEEM trace, obtained after complete $^1H\backslash^2H$ exchange, compared to a similar set of calculated data as shown in Figure 5: one and two coupled deuterons with average T_{dip} equal to 0.22 and 0.54 MHz. A direct comparison between the two experimental traces in Figures 5 and 9 shows that the Y_Z site has an exchangeable ^1H occupancy that depends on the presence or absence of the $(Mn)_4$

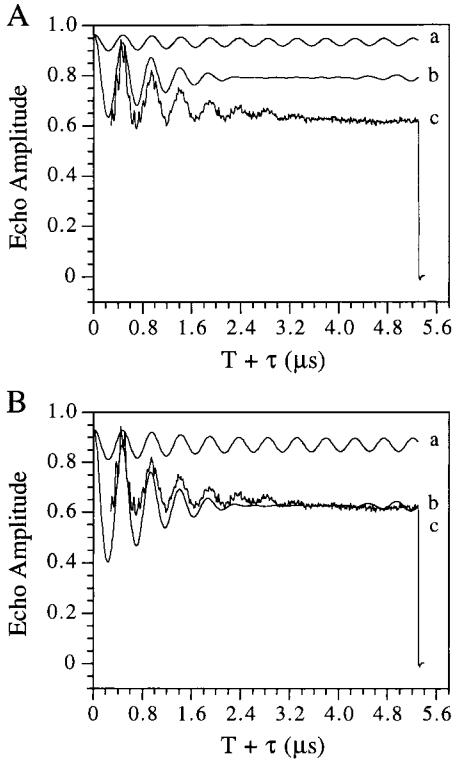

Figure 9. Three-pulse ESEEM representing $Y_Z^\bullet$ in Mn-depleted samples compared to simulations. The $Y_Z^\bullet$ time-domain data (trace c) are the same as shown in Figure 6C. The simulated traces represent (A) one ^{2}H nucleus with a T_{dip} of (a) 0.22 and (b) 0.54 MHz and (B) two ^{2}H nuclei with T_{dip} equal to (a) 0.22 and (b) 0.54 MHz. Simulation parameters: H_0 3247 G; τ 235 ns; A_{iso} 0 MHz; e^2qQ 0.25 MHz; η 0.

cluster. In contrast to $S_2Y_Z^\bullet$ in Ca-depleted PSII, the trace representing $Y_Z^\bullet$ in the Mn-depleted samples shows shallow and more long-lived modulations. The data in Figure 9 indicate that, as opposed to $S_2Y_Z^\bullet$ in Ca-depleted PSII, only one moderately strong ^{2}H coupling might be involved. In addition, the decreased modulation depth and the persistence of the ^{2}H modulations for >3 μs indicate that there is a substantial contribution from weakly coupled ^{2}H in the $Y_Z^\bullet$ trace. As for the Ca-depleted system, the coarse comparison between experimental and simulated data shown in Figure 9 was followed by a more detailed simulation analysis. A calculated ESEEM trace, which includes one deuteron with a T_{dip} of 0.40 MHz (^{1}H 2.61 MHz) and 3 deuterons coupled with an average T_{dip} of 0.24 MHz (^{1}H 1.56 MHz), is overlaid on the $Y_Z^\bullet$ trace in Figure 6C. The corresponding frequency spectra are shown in Figure 7B. Spectral features consistent with heterogeneous hydrogen bonding of $Y_Z^\bullet$ and a general disorder in the site have been reported for Mn-depleted samples and, consequently, these numbers do not necessarily represent a unique solution to the $Y_Z^\bullet$ ESEEM data (e.g. refs 12 and 69). Nonetheless, although minor variation in the hf couplings may be present, the modulation depth and the damping of the $Y_Z^\bullet$ ESEEM data are consistent with one more strongly interacting deuteron and, in addition, several weakly coupled deuterons.

We estimate, with the signal-to-noise of our data, that the changes in $Y_Z^\bullet$ environment observed in the two cofactor-depleted systems occur within a 4−4.5 Å radius from the magnetic center of the radical. We note that we do not attempt to fit the rapid modulations from the nonexchangeable ^{1}H nuclei that ride on top of the slower ^{2}H modulations, as is clearly seen in the experimental data in Figures 5−9.

Discussion

Radical Yield and Spectral Quality. We have been able to trap 70% of the transient $Y_Z^\bullet$ species in samples devoid of the essential cofactors Mn, Ca^{2+}, and Cl^-. The cryotrapping protocol used for $Y_Z^\bullet$ in the Mn-depleted PSII samples in this work is similar, but not identical, to those described earlier for samples from spinach[26a,34] and from *Synechocystis* 6803.[26b] In terms of trapping yield, the amount of $Y_Z^\bullet$ trapped by Kawamori and co-workers is difficult to evaluate, as they used a 30 min annealing period to obtain the pure $Y_D^\bullet$ spectrum, which was used as the spin standard. $Y_D^\bullet$ is likely to decay during this relatively long dark adaptation, which could produce errors in the spin quantification. In the work here, the samples containing the trapped $Y_Z^\bullet$ radical were thawed and incubated for 2 mins in darkness. The $Y_Z^\bullet$ decay is quantitative during the annealing period, but $Y_D^\bullet$ is stable, which allows us to obtain an accurate $Y_Z^\bullet$ spin concentration. For the *Synechocystis* samples, Diner and co-workers reported trapping $Y_Z^\bullet$ at close to one per reaction center. The higher trapping yield in *Synechocystis* may reflect the slower P_{680}^+/Q_A^- charge-recombination rate in cyanobacteria relative to higher plants.[7b]

$Y_D^\bullet$ and Chl^+ radicals give rise to signals that overlap the $Y_Z^\bullet$ spectrum and could interfere with ESEEM measurements on Mn-depleted samples. We avoided contamination by $Y_D^\bullet$ in the light-minus-annealed data by maintaining the concentration of $Y_D^\bullet$ constant in the light and dark-annealed samples. Our trapping procedure was optimized to avoid Chl^+ species, as indicated by the pure $Y_Z^\bullet$ spectrum shown in Figure 1A. As a result, the ESEEM traces were reproducible at different field positions within the $Y_Z^\bullet$ EPR spectrum, which would not be the case if narrow Chl^+ signals were present under the broader $Y_Z^\bullet$ line shape.

For the Ca-depleted system, neither $Y_D^\bullet$ nor Chl^+ caused concern, as the ESEEM data were recorded in the wings of the broad $S_2Y_Z^\bullet$ spectrum, and therefore, outside the EPR spectra of these radicals. For background subtraction in the Ca-depleted samples, the multiline signal became fully induced during the preparation and ^{1}H\/^{2}H-exchange procedures and formed a dark-stable state.[33,45,56] Signals from other metal centers (see Figure 1B) have broad line shapes and low amplitudes; consequently, their spectral contributions are weak. Small differences in amplitude between the light and dark spectrum are observed for cytochrome b_{559}. These changes are, however, negligible as compared to the amplitude of the $S_2Y_Z^\bullet$ spectrum. We conclude that EPR signals form sources other than $S_2Y_Z^\bullet$ in our samples provided a stable background and their spectral contribution could be efficiently subtracted.

At the outset, ESEEM measurements were performed on both the low-pH treated and the NaCl/EDTA-washed material. The low-pH prepared samples, however, were better suited for a detailed characterization, as this material, which contained the three extrinsic subunits, was more resistant to Mn release and the resulting spectral contaminations from hexaaquo Mn^{2+} species.

Hydrogen Bonding of Y_Z. The ESEEM analysis on $Y_Z^\bullet$ in Mn-depleted samples revealed hf interaction to a single ^{2}H nucleus with T_{dip} of 0.40 MHz (^{1}H 2.61 MHz). If we make the reasonable assumption that the 0.40 MHz coupling occurs to the tyrosine oxygen, which carries a spin density of 0.28,[12,50] the calculated distance of 2.04 Å between the two nuclei suggests a hydrogen bond interaction. Several studies indicate that the H-bonding partner to Y_Z is D1-H190, as this residue is essential for Y_Z function.[70,71] Retardation in Y_Z oxidation by P_{680}^+ is observed in all D1-H190 mutants reported, and the usual

phenotype is complete inactivation of water oxidation. Assembly of a functional $(Mn)_4$ cluster and low rates of oxygen evolution are only detected upon changing the histidine to an arginine or a lysine.[70d,71] These data point to the acid−base properties of D1-H190 as its key functional role in PSII and suggest that this residue is the initial proton acceptor upon Y_Z oxidation, as discussed in detail elsewhere.[9,20] In agreement with this interpretation, optical studies on Mn-depleted samples have shown that the electron- and proton-transfer reactions associated with Y_Z redox chemistry are modulated by a base with a pK_a consistent with that of a histidine.[19,72,73] Finally, analogies to the D2 side suggest a close Y_Z\D1-H190 interaction, as the H-bonding partner to Y_D is D2-H189.[67b,74]

Hydrogen bonding to $S_2Y_Z^\bullet$ in samples that retain the $(Mn)_4$ cluster, but lack Ca^{2+}, is clearly distinct from $Y_Z^\bullet$ in samples devoid of both metal ions. The electron spin $^1/_2$, nuclear spin 1 ESEEM analysis of $S_2Y_Z^\bullet$ in the Ca-depleted system is consistent with two interacting ^{2}H nuclei with T_{dip} of 0.48 ± 0.04 MHz. The presence of two deuterons with similar hf couplings suggests a bifurcated H bond to the oxygen of the tyrosine headgroup, as has been proposed for $S_2Y_Z^\bullet$ in acetate-treated PSII based on studies similar to those described here (but see also ref 23c).[21] With this assumption, the observed hf couplings correspond to dipolar distances around 1.92 Å. One of the H-bond donors to $Y_Z^\bullet$ in Ca-depleted PSII is likely to be D1-H190. The second donor may be substrate water ligated to the $(Mn)_4$ cluster or an endogenous protein donor, as discussed below.

Solvent Accessibility to the Y_Z Site. Regardless of the integrity of the OEC, ^{1}H\$^2$H-isotope exchange occurs on the hour time scale at the Y_D site, as shown in earlier studies[67] and verified here. For the Y_Z site, however, the ^{1}H\$^2$H exchange is completed more rapidly, with an upper limit of ∼35 min, in both Mn-depleted[75] and Ca-depleted samples (Figures 3 and 4). Thus, although Y_Z and Y_D are expected to lie at the same depth in the thylakoid membrane,[76] there is a substantial variance in the water accessibility to the two tyrosines. On the basis of more indirect evidence, a similar conclusion was made from cw-ENDOR studies on $Y_Z^\bullet$ and $Y_D^\bullet$ in Mn-depleted PSII.[26b]

Our results show that ^{1}H\$^2$H exchange at Y_Z occurs within minutes or faster in the absence or presence of the $(Mn)_4$ cluster, consistent with the metalloradical mechanism for water oxidation. There is, however, a marked difference in the number of exchangeable protons detected in the vicinity of $Y_Z^\bullet$ as a function of the integrity of the Mn site. The ESE characterization of $Y_Z^\bullet$ in Mn-depleted PSII revealed hf interactions to several weakly coupled deuterons with a T_{dip} of ∼0.24 MHz (^{1}H 1.56 MHz). Within a simple point-dipole model, a 0.24 MHz interaction translates into a radial distance of about 3.7 Å between $Y_Z^\bullet$ and the incorporated ^{2}H nuclei. We did not observe similar weak hf interactions in Ca-depleted samples. These results suggest that Y_Z is more shielded from the solvent in the Ca-depleted system and, upon removal of the $(Mn)_4$ cluster, that bulk water enters the site. Alternatively, carboxylates in the $(Mn)_4$ binding site that normally ligate the metal ions may become protonated from bulk as the manganese is extracted. In any event, the spin−echo data indicate a more solvent accessible site in the absence of the metal center. Rigid control of the accessibility to the Y_Z site in the presence of the $(Mn)_4$ cluster is consistent with the long lifetime of $S_2Y_Z^\bullet$ in Ca-depleted PSII, on the order of seconds, and its relative insensitivity to externally added reductants.[39] In contrast, $Y_Z^\bullet$ decays on the millisecond time scale in Mn-depleted samples and, upon addition of exogenous reductants, is reduced with fast second-order kinetics indicating close approach.[36,37,66b,77] In addition, thermal melting of the $Y_Z^\bullet$ site in Ca-depleted samples exhibits a highly cooperative transition with a T_m ∼50 °C lower than that in Mn-depleted samples.[78] The relatively uncooperative melting process and high T_m in the absence of the $(Mn)_4$ cluster support the finding here that bulk water has access to the Y_Z site in this system.

Y_Z Deprotonation and Chlorophyll Optical Absorption Bandshifts in Mn-Depleted PSII. The metalloradical mechanism for water oxidation postulates that Y_Z deprotonates through the protein matrix to bulk solvent upon its oxidation by P_{680}^+. Consistent with this proposal, $Y_Z^\bullet$ is a neutral radical[11] and optical measurements on Mn-depleted samples detect proton release and uptake upon oxidation and reduction of Y_Z, respectively.[19,72,79] In dispute, however, is whether these data indicate that the local, redox-driven acid/base chemistry in the Y_Z site equilibrates with the bulk medium through the protein matrix to give rise to the observed pH transients. An alternative interpretation is that the proton released upon Y_Z oxidation remains locally trapped in the site and that a charge is created, which gives rise to electrostatic shifts in the pK_a's of peripheral amino acids.[18,19] Upon rereduction of $Y_Z^\bullet$ in this model, the locally trapped proton reassociates with the phenol, the charge is quenched, and the peripheral amino acids relax to their original pK_a's.

The spin−echo results on Mn-depleted preparations above support the notion that the proton release/uptake observed in the bulk medium in response to redox changes at Y_Z is chemically induced rather than of electrostatic origin, as they show that the perturbed water-splitting site is in facile contact with solvent. Several other points also argue in favor of $Y_Z^\bullet$ equilibration through the protein matrix with the bulk phase. The ready access of external reductants to $Y_Z^\bullet$ in the absence of the $(Mn)_4$ cluster has been mentioned above. Moreover, if a charge were retained in the $Y_Z^\bullet$ site, there would be substantial energetic consequences associated with stabilizing it in the low dielectric protein medium. Consideration of the $Y_Z^\bullet/Y_Z$ reduction potential relative to the midpoint potential of P_{680}^+ indicates that there is little excess driving force in the $Y_ZP_{680}^+ \rightarrow Y_Z^\bullet P_{680}$ reaction.[3] Accordingly, the source of the additional energy necessary to stabilize the hypothesized local charge is problematic. These energetic concerns are reinforced by recent density functional calculations that indicate that removing the proton from the site is essential for effective Y_Z oxidation by

(70) (a) Diner, B. A.; Nixon, P. J.; Farchaus, J. W. *Curr. Opin. Struct. Biol.* **1991**, *1*, 546−554. (b) Nixon, P. J.; Diner B. A. *Biochem. Soc. Trans.* **1994**, *22*, 338−343. (c) Roffey, R. A.; Kramer, D. M.; Govindjee; Sayre, R. T. *Biochim. Biophys. Acta* **1994**, *1185*, 257−270. (d) Chu, H.-A.; Nguyen, A. P.; Debus, R. J. *Biochemistry* **1995**, *34*, 5839−5858.

(71) Hays, A.-M. A.; Vassiliev, I. R.; Golbeck, J. H.; Debus, R. J. *Biochemistry* **1998**, *37*, 11352−11365.

(72) Rappaport, F.; Lavergne, J. *Biochemistry* **1997**, *36*, 15294−15302.

(73) Conjeaud, H.; Mathis, P. *Biophys. J.* **1986**, *49*, 1215−1221.

(74) (a) Tommos, C.; Davidsson, L.; Svensson, B.; Madsen, C.; Vermaas, W.; Styring, S. *Biochemistry* **1993**, *32*, 5436−5441. (b) Campbell, K. A.; Peloquin, J. M.; Diner B. A.; Tang, X.-S.; Chisholm, D. A.; Britt, R. D. *J. Am. Chem. Soc.* **1997**, *119*, 4787−4788.

(75) The observation of complete ^{1}H\$^2$H exchange on the minutes time scale at the Y_Z site in the Mn-depleted system is consistent with optical measurements on ^{1}H\$^2$H-isotope effects on the reduction rate of P_{680}^+ (Diner, B. A. Unpublished. Lydakis-Simantiris, N.; Babcock, G. T.; Golbeck, J. Unpublished.).[19]

(76) (a) Innes, J. B.; Brudvig, G. W. *Biochemistry* **1989**, *28*, 1116−1125. (b) Isogai, Y.; Itoh, S.; Nishimura, M. *Biochim. Biophys. Acta* **1990**, *1017*, 204−208. (c) Koulougliotis, D.; Tang, X.-S.; Diner, B. A.; Brudvig, G. W. *Biochemistry* **1995**, *34*, 2850−2856.

(77) Babcock, G. T.; Ghanotakis, D. F.; Ke, B.; Diner, B. A. *Biochim. Biophys. Acta* **1983**, *723*, 276−286.

(78) Tommos, C.; Dorlet, P.; Babcock, G. T. Manuscript in preparation.

(79) Renger, G.; Voelker, M. *FEBS Lett.* **1982**, 149, 203−207.

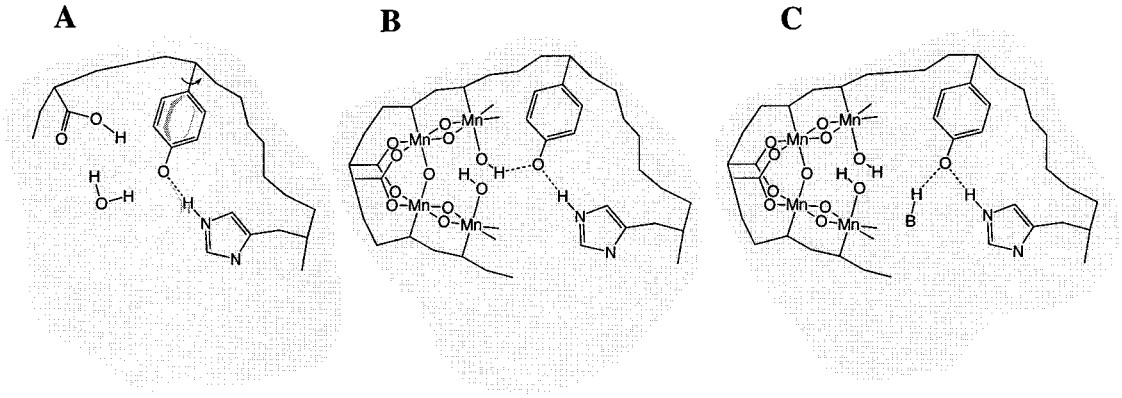

Figure 10. Summary of the environment and hydrogen bonding of $Y_Z^\bullet$ in (A) Mn-depleted PSII and in (B, C) Ca-depleted PSII (see text for details). The gray shading in each of the panels indicates diffusion barriers for protonic contact with bulk phase.

P_{680}^+.[80] Overall, there is a reasonable body of data that suggests that proton release upon formation of $Y_Z^\bullet$ equilibrates rapidly with the bulk phase, although there appears to be a preparation-dependent diffusion barrier through the protein that affects the kinetics observed.[72,79]

In support of the electrostatic model for the observed pH transients upon redox change at Y_Z, however, are optical absorption bandshifts in PSII chlorophyll(s) that accompany the tyrosine redox changes. Several groups have argued that these bandshifts arise as the result of the postulated retained positive charge.[19,72,81] The interpretation of these bandshifts as reflecting an electrostatic, as opposed to a chemical, origin, however, is ambiguous and compromised by the facts that neither the extent nor the kinetics of proton release correlates with the amplitude and kinetics of the chlorophyll bandshifts.[19,72] The pigment absorption changes follow the redox state of Y_Z closely, which suggests that a shift in a local interaction of a chlorophyll pigment may be coupled to the Y_Z redox cycle.[20e] If, for example, a weak hydrogen bond to the 9-keto carbonyl of a chlorophyll became stronger upon oxidation of Y_Z and relaxed upon its reduction, red shifts in both the Soret and Q_y region of the chlorophyll would occur and correlate with electron transfer through Y_Z. Recent FTIR work by Wydrzynski and co-workers indicates that this situation may indeed hold.[82] Briefly, they showed that the oxidation of Y_Z is accompanied by a large differential band at 1706/1699 cm^{-1}. As tyrosine modes are not expected in this region, they attributed the vibrational shift to the keto group of a chlorophyll. Such a shift in ν(C=O) is characteristic of a change in H-bond strength,[83] which suggests that the H-bonding interaction and hence the optical absorption spectrum of the chlorophyll are coupled to the redox state of Y_Z. These data provide a means by which to rationalize the chlorophyll bandshifts without the necessity of postulating a charge in the $Y_Z^\bullet$ site.[20e]

The question above as to the equilibration of the Y_Z site with bulk solvent is pertinent of the light-driven assembly mechanism of the OEC.[27] In other metalloenzymes, the extent of exposure of the apoenzyme active site and the metal incorporation process vary widely.[84] In apo-ribonucleotide reductase (apo-RNR) and in apo-plastocyanin (apo-PC), for example, the structure of the enzyme in the apo-state is not significantly perturbed from the holoenzyme and structural fluctuations in the protein to allow metal incorporation are thought to be necessary.[85] In other proteins, for example, lactoferrin and hemerythrin, the native enzyme structure is dependent upon the presence of the metal and, in its absence, the empty metal site is exposed to solvent.[86]

The behavior of the apo-PSII appears to be more similar to that of apo-RNR and apo-PC, as access from bulk to the metal-depleted $Y_Z^\bullet$ site occurs, but appears to be kinetically limited. This suggests that local fluctuations in the Y_Z environment are required to allow Mn^{2+} and Ca^{2+} access from the bulk phase. Recent detailed studies on the photoactivation process suggest that the metal ion incorporation proceeds relatively slowly and may rate limit the process.[87] The proton equilibration data support this notion as the release/uptake kinetics that follows the Y_Z redox cycle in Mn-depleted samples vary depending on the specifics of the preparation.[19,72] Moreover, effective oxidation of Y_Z by P_{680}^+ in the absence of the $(Mn)_4$ cluster still requires the presence of D1-H190. Neither of these phenomena would be expected if the site were directly open to solvent. Finally, the recent chemical rescue work reported by Debus and co-workers indicates that imidazole, added to the bulk phase, can restore both Y_Z oxidation by P_{680}^+ and $Y_Z^\bullet$ recombination with Q_A^- in D1-H190 mutants.[71] The second-order rate constant for this process is on the order of 10^5 M^{-1} s^{-1}, indicating that the entry of imidazole into the active site is not diffusion limited, which points to protein structural fluctuations as limiting the overall process. Taken together, the spin−echo results and the considerations above suggest that the $Y_Z^\bullet$ site equilibrates rapidly with bulk phase in the absence of the $(Mn)_4$ cluster, but that this equilibration is rate-limited by local protein fluctuations.

Cofactor-Dependent Structure of the Y_Z Site. Figure 10 summarizes the Y_Z site as a function of the metal composition of the OEC. Figure 10A shows the Y_Z structure and environment in the $Ca^{2+}/(Mn)_4$-depleted system. For the Ca-depleted system, two possible H-bonding arrangements are shown in Figure 10, parts B and C. Independent of the status of the metal

(80) Blomberg, M. R. A.; Siegbahn, P. E. M.; Babcock, G. T. *J. Am. Chem. Soc.* In press.

(81) Diner, B. A.; Tang, X.-S.; Zheng, M.; Dismukes, G. C.; Force, D. A.; Randall, D. W.; Britt, R. D. In *Photosynthesis: from Light to Biospere*; Mathis, P., Eds.; Kluwer Academic Publishers: The Netherlands, 1995; Vol. II, pp 229−234.

(82) Zhang, H.; Razeghifard, M. R.; Fischer, G.; Wydrzynski, T. *Biochemistry* **1997**, *36*, 11762−11768.

(83) Babcock, G. T.; Callahan, P. M. *Biochemistry* **1983**, *22*, 2314−2319.

(84) *Mechanisms of Metallocenter Assembly*; Hausinger, R. P., Eichhorn, G. L., Marzilli, L. G., Eds.; VCH Publishers: New York, 1996.

(85) (a) Åberg, A.; Nordlund, P.; Eklund, H. *Nature* **1993**, *361*, 276−278. (b) Garrett, T. P. J.; Clingeleffer, D. J.; Guss, J. M.; Rogers, S. J.; Freeman, H. C. *J. Biol. Chem.* **1984**, *259*, 2822−2825.

(86) (a) Anderson, B. F.; Baker, H. M.; Norris, G. E.; Rumball, S. V.; Baker, E. N. *Nature* **1990**, *344*, 784−787. (b) Kurtz, D. M., Jr. In *Mechanisms of Metallocenter Assembly*; Hausinger, R. P., Eichhorn, G. L., Marzilli, L. G., Eds.; VCH Publishers: New York, 1996; pp 19−40.

(87) Zaltsman, L.; Ananyev, G. M.; Bruntrager, E.; Dismukes, G. C. *Biochemistry* **1997**, *36*, 8914−8922.

cluster, Y_Z is most likely H bonded to D1-H190 in both its reduced and oxidized form, as discussed above.

In Mn-depleted PSII, Figure 10A, hydrogen bonding to $Y_Z^\bullet$ spans a range of geometries and the position of its phenol headgroup is disordered.[12,26,59,69] In addition, the site is in equilibrium with the bulk phase and water molecules and/or protonated carboxyl groups, which ligate the $(Mn)_4$ cluster in the holoenzyme, are present in the direct vicinity of the tyrosine. During assembly of the $(Mn)_4$ cluster, the carboxylate ligands must deprotonate, which accounts for the observation of proton ejection during the cluster assembly.[27d] The accessibility of Y_Z to the bulk medium in Mn-depleted PSII may rationalize observations that have been interpreted to indicate that Y_Z is not H bonded to D1-H190 in its radical form. Point-mutations at D1-H190 do not perturb the cw-EPR spectrum of $Y_Z^\bullet$ to any significant extent[88] in contrast to mutations introduced at D2-H189, which abolish or severely perturb the EMR features of $Y_D^\bullet$.[20c,67b,74] The studies on the D1-H190 mutants, however, were performed on samples that did not contain the $(Mn)_4$ cluster. In light of the results shown here, we suggest that bulk water, present in the Y_Z site, can replace, although not in a kinetically competent fashion, D1-H190 as the proton acceptor.

In the proposed hydrogen-abstraction models, $(Mn)_4Y_Z$ forms a single structural and functional unit and, within the framework of this model, Y_Z is expected to be disordered in the absence of the metal cluster. Moreover, on the basis of photoactivation arguments, solvent should be detectable in the immediate vicinity of Y_Z. Both of these predictions are consistent with the experimental observations. Binding of Mn^{2+} and Ca^{2+} ions and assembly of the $(Mn)_4$ cluster are likely to increase order in the active site and impose rigid control of its accessibility to bulk water. Although our studies are restricted to the Ca-depleted system, a decrease in accessibility to $Y_Z^\bullet$ in samples that contain the $(Mn)_4$ cluster is observed. In addition, the cooperative melting of the $Y_Z^\bullet$ site in Ca-depleted PSII, relative to the Mn-depleted system, suggests a more homogeneous Y_Z environment in the presence of the $(Mn)_4$ cluster.[78]

The predictions from the metalloradical model made above are fairly general and do not necessarily require that Y_Z functions as a H-atom abstractor. Nonetheless, our results in the Mn-depleted samples relative to the Ca-depleted enzyme reveal a sensitivity of the Y_Z site to the removal of the $(Mn)_4$ cluster that is consistent with an intimate relationship between the two redox cofactors. This is also reflected in the thermodynamic and kinetic properties of Y_Z, which depend on the redox and compositional state of the OEC metal site. The midpoint potential of Y_Z varies as a function of the S states,[3] and upon removal of the $(Mn)_4$ cluster, is decreased by 50−120 mV in the pH range 5−8.5.[89] Moreover, the oxidation and reduction rates of Y_Z vary dramatically as a function of sample preparation, the status of the extrinsic subunits, and the composition of the metal cluster.[e.g.38,90]

A more specific prediction of our mechanistic model is that Y_Z is involved in two hydrogen bonds during the catalytic cycle (see also ref 21).[9] One of these H bonds is to D1-H190, which serves as the first residue in a proton-transport pathway through the protein matrix that eventually leads to the bulk medium. The second H-bonding partner is predicted to be substrate coordinated to the $(Mn)_4$ cluster in the intact system. Figure 10, parts B and C, displays possible structural arrangements of the Y_Z site in the $S_2Y_Z^\bullet$ state of the Ca-depleted enzyme. $Y_Z^\bullet$ may be involved in a bifurcated H bond to D1-H190 and to one of the substrate molecules coordinated to the catalytic Mn ions (Figure 10B) or, alternatively, to some other base in the vicinity of the tyrosine (Figure 10C). The structures shown in Figure 10, parts B and C, are consistent with a $(Mn)_4-Y_Z^\bullet$ center-to-center distance around 8 Å.[23] Moreover, parts B and C in Figure 10 are in agreement with the fact that we detect only two exchangeable ^2H nuclei, since the upper limit for detection of a single ^2H coupled to the tyrosine oxygen is about 3.0 Å within the signal/noise of our data.

As discussed earlier, the Ca-depleted PSII enzyme is inhibited after formation of the $S_2Y_Z^\bullet$ state. If the contact between $Y_Z^\bullet$ and substrate is broken, as illustrated in Figure 10C, the reason for the inhibition is clear. If, however, the structure shown in Figure 10B more accurately describes the system, other reasons for the inhibition have to be considered. Hydrogen atom transfer rates dependent on the potential surface that describes the donor−acceptor system. Owing to the relatively large mass of the proton compared to the electron, a minor shift in the distance that separates the donor and acceptor will have a significant effect on the H-atom tunneling rate.[91] Thus, it is possible that Ca^{2+} depletion perturbs the $(Mn)_4Y_Z$ structure sufficiently to block the normal S cycle. Alternatively, in Ca-depleted PSII, the $(Mn)_4Y_Z$ structure and the positioning of the substrate may be close to native, but a normal S_2 state cannot be formed owing to changes in the reduction potentials of the redox cofactors and/or the bond-dissociation energies of the substrates.

Acknowledgment. We acknowledge valuable discussions with Marilena di Valentin, Rick Debus, Pierre Dorlet, and Nikos Lydakis-Simantiris and we thank Pierre Dorlet and Catherine DeMaso for SDS-PAGE analysis. This work was supported by NIH Grant GM 54065 to J.McC.; USDA Competitive Research Grants Program, Human Research Frontiers Program and NIH Grant GM 37300 to G.T.B.; and the Swedish Natural Science Research Council and the Knut and Alice Wallenberg Foundation to S.S.

JA980281Z

(88) (a) Roffey, R. A.; van Wijk, K. J.; Sayre, R. T.; Styring, S. *J. Biol. Chem.* **1994**, *269*, 5115−5121. (b) Bernard, M. T.; MacDonald, G. M.; Nguyen, A. P.; Debus, R. J.; Barry, B. A. *J. Biol. Chem.* **1995**, *270*, 1589−1594.

(89) (a) Yerkes, C. T.; Babcock, G. T.; Croft, A. R. *FEBS Lett.* **1983**, 158, 359−363. (b) Buser, C. A.; Thompson, L. K.; Diner, B. A.; Brudvig, G. W. *Biochemistry* **1990**, *29*, 8977−8985.

(90) Razeghifard, M. R.; Wydrzynski, T.; Pace, R. J.; Burnap, R. L. *Biochemistry* **1997**, *36*, 14474−14478.

(91) Cha, Y.; Murray, C. J.; Klinman, J. P. *Science* **1989**, *243*, 1325−1330.